Full Bicycle Dynamic Model for Interactive Bicycle Simulator

Qichang He
Xiumin Fan
Dengzhe Ma

CIM Institute,
School of Mechanical and Power Engineering,
Shanghai Jiaotong University,
Shanghai, China, 200030

An interactive bicycle simulator with six degrees of freedom motion system could bring the rider a very realistic riding feeling. An important component of the simulator is the full bicycle dynamic model that simulated the two-wheeled bicycle dynamics. It consists of two slightly coupled submodels: The stability submodel and the vibration submodel. The stability submodel solves the stability of the bicycle under rider's active maneuvers and the vibration submodel evaluates the vibration response of the bicycle due to uneven road surface. The model was validated by several experiments and successfully applied to the interactive bicycle simulator. [DOI: 10.1115/1.2121749]

Keywords: interactive bicycle simulator, bicycle dynamic model, the stability sub-model, the vibration sub-model

1 Introduction

Many motion-based simulators have been developed for different types of vehicles, such as flight, car, and motorcycle. Among them, the flight simulator is the most successful one, followed by the driving simulator for road vehicles. In the field of motion-based bicycle simulators, only a few studies have been conducted. To the authors' knowledge only the Korea KAIST interactive bicycle simulator and the Singapore NTU bicycle simulator [both with a six degrees of freedom (DOF) motion platform] have been studied and developed [1].

We also developed an interactive bicycle simulator that is very similar to the Korea KAIST bicycle simulator in hardware, as shown in Fig. 1. It is based on a motion generation system consisting of a Stewart platform to provide 6 DOF motions, handlebar and pedal resistance system which are attached to the handlebars and the rear wheel, respectively, to provide force feedback; a PowerWall virtual reality (VR) system includes three Barco® projectors to create a realistic virtual riding scene and a Yamaha® three-dimensional sound system to produce environmental sound. It can give the rider on board the impression that he/she rides an actual bicycle and feeding back corresponding visual, audio, and motion cues to the rider. Also in the simulator, the rider experiences the same physical sensations as those perceived during the riding of a real bicycle on various roads. This is valid not only in terms of perceived sense of movements, accelerations and decelerations, and control movements of a bicycle, but also for the bicycle's pedal and handlebar force feedback arising from the road condition such as upgrade and downgrade. The characteristics of the bicycle simulator become very similar to that of an actual bicycle.

A simplified control flow of a bicycle simulator is sketched in Fig. 2. The bicycle dynamic model (BDM) is the most important component in the software system of an interactive bicycle simulator. The BDM solves in real-time motion equations written for the geometrical, inertial, and mechanical characteristics of the road-bicycle-rider system. The rider's maneuvers and the inputs from virtual scene, such as road profile and wind resistance, are sampled and fed to the BDM that compute the dynamics response of a bicycle. The bicycle motion is then processed by the motion generation system which brings the real motion cues to the rider on a simulator.

The visual elegance and mechanical simplicity of a bicycle belie its surprising complex dynamics, especially concerning the road-bicycle-rider system. The inherent unstable dynamics of the bicycle coupled with the rider's dynamics and uneven road make the bicycle dynamics more complex. In this paper, a full BDM adopted in our bicycle simulator is presented. It includes a stability submodel and a vibration submodel, which fully describe the bicycle dynamics accounting for tire flexibility, road profile and rider's pedal and handlebar and tilt inputs.

2 Bicycle Dynamic Model

2.1 Whole Scheme of Bicycle Dynamic Model. On the basis of the theory of analytical mechanics, we developed the following full dynamic model to describe the dynamics of complex rider-bicycle-road system. The whole scheme of the BDM for the bicycle simulator is shown in Fig. 3. It has three torque estimators, one stability submodel, and one vibration submodel. Just as their names imply, torque estimators get input torques for the dynamics submodels from the bicycle simulator system; the stability submodel evaluates the stability of the bicycle under the rider's maneuvers; the vibration submodel solves the vibration response of a bicycle induced by the unevenness of the road surface. The outputs are the positions, velocities, and accelerations of a bicycle.

The stability submodel and the vibration submodel are slightly coupled by the velocity of a bicycle. In Fig. 3, the velocity of bicycle computed by the stability submodel will be input to the vibration submodel to evaluate the vibration response of a bicycle due to the unevenness of the road surface. It is known that the variation of vibration stress on the rider mainly depends on the velocity when the road surface is the same. We only consider the velocity as the coupled variable in order to simplify the model.

2.2 Stability submodel. The bicycle has some degrees of self-stability which has been analyzed for many times from different mathematical levels in previous studies, such as Jones [2], Lowell [3], Fajans [4], and Hand [5]. Among them, Hand [5] has thoroughly derived the motion equations for a bicycle using a Lagrangian method and done numerical simulations of bicycle dynamics based on these equations. In this study, we developed our stability submodel based on Hand's work, but considering much more complex riding maneuvers. The rider can lean his/her body and steer the handlebar to control the stability of the bicycle; also he/she can pedal the bicycle and make the velocity of the bicycle changeable. Our research aims at eliminating ideal riding behaviors of Hand's work, and makes the rider on a bicycle simulator get a more realistic riding feeling. To build the stability model we make almost the same simplifying assumptions about

Contributed by the Application Track Committee for publication in the JOURNAL OF COMPUTING AND INFORMATION SCIENCE IN ENGINEERING. Manuscript received June 8, 2004; final manuscript received October 31, 2004. Assoc. Editor: S. Szykman.

Fig. 1 Interactive bicycle simulator

the bicycle-rider system and its behavior as Hand's work, but we do not assume the bicycle run on a rigid horizontal surface and the rider can control the bicycle through pedaling, steering, and leaning.

The following seven independent generalized coordinates are used to describe the bicycle's position and orientation at any time: X_r, Y_r, χ_r, θ_r, ψ, ϕ_f, ϕ_r. Once these generalized coordinates are specified, the position and orientation of the bicycle can be defined accurately at any given time with respect to the inertial coordinate system. A sketch of the seven independent generalized coordinates and four auxiliary variables $(X_f, Y_f, \chi_f, \theta_f)$ is shown in Fig. 4. The auxiliary variables can be expressed by the generalized coordinates. All angles in Fig. 4 are indicated with their positive direction. The basic parameters used to specify the bicycle geometry are shown in Fig. 5.

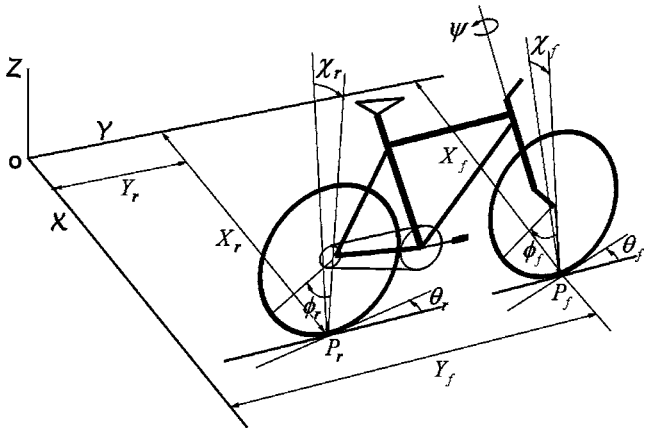

Fig. 4 Generalized and auxiliary coordinates of stability submodel

Based on these generalized coordinates, we can establish formulas to calculate the kinetic energy and potential energy of the bicycle system. To simplify calculation of the bicycle kinetic energy, the bicycle system is divided into two separate parts; the rear and front. The rear part includes bicycle frame, rider, and rear wheel. The front part includes the handlebar assembly and front wheel. We notice that the rear wheel can only rotate relative to the bicycle frame; therefore, the bicycle frame and the rear wheel can be treated as one rigid body for the calculation of translational kinetic energy of the rear part T_r^{trans}. Similarly, we can calculate the rotational kinetic energy of the rear part T_r^{rot} by treating the rear wheel as if it was rigidly attached to the bicycle frame, and then add the additional rotational kinetic energy $T_{\text{rwheel}}^{\text{spin}}$ due to the spinning of the rear wheel relative to the rear frame [5]. The kinetic energy of the front part is very similar to the rear part, except for the generalized coordinates to auxiliary variables. The following formulas show the bicycle kinetic energy and the potential energy

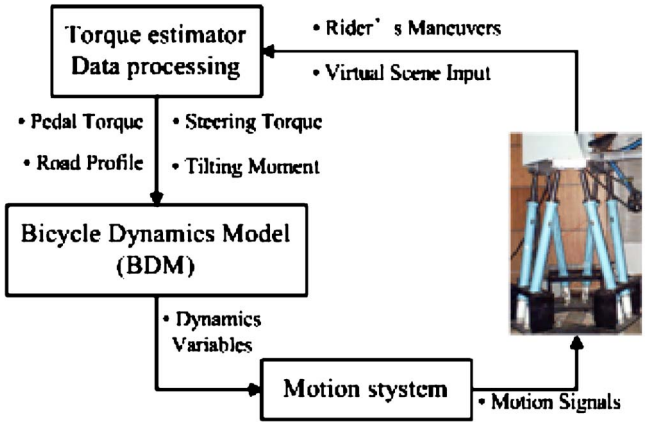

Fig. 2 Control flow of interactive bicycle simulator

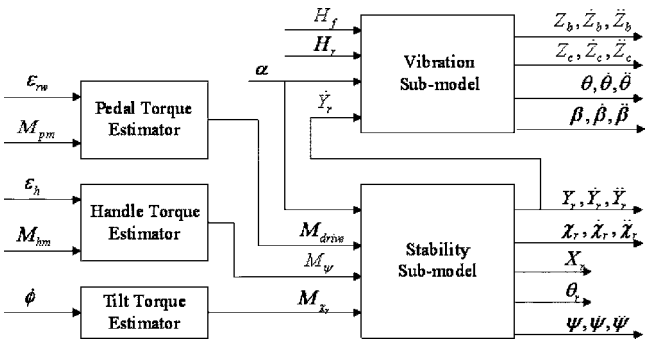

Fig. 3 The whole scheme of bicycle dynamic model

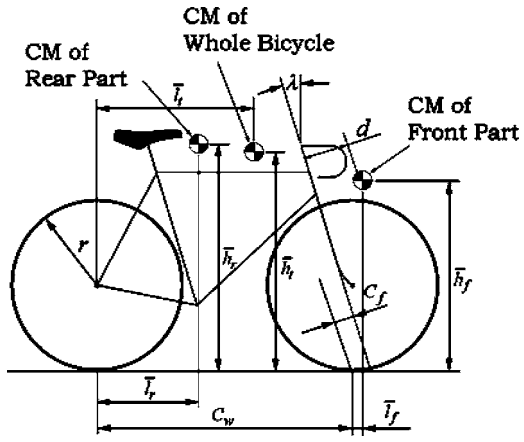

Fig. 5 Basic parameters of stability submodel

$$T_r = \overbrace{\frac{1}{2}m_r(\dot{X}_r - \bar{l}_r\dot{\theta}_r + \bar{h}_r\dot{\chi}_r)^2 + \frac{1}{2}m_r\dot{Y}_r^2}^{T_r^{\text{trans}}} + \overbrace{\frac{1}{2}(R_{\overline{yy}}\dot{\chi}_r^2 + 2R_{\overline{yz}}\dot{\chi}_r\dot{\theta}_r + R_{\overline{zz}}\dot{\theta}_r^2)}^{T_r^{rot}} + \overbrace{\frac{1}{2}J_r\dot{\phi}_r^2 + J_r\dot{\phi}_r\dot{\theta}_r\chi_r}^{T_{\text{rwheel}}^{\text{spin}}} \quad (1)$$

$$T_f = \overbrace{\frac{1}{2}m_f(\dot{X}_f - \bar{l}_f\dot{\theta}_f + \bar{h}_f\dot{\chi}_f)^2 + \frac{1}{2}m_f\dot{Y}_f^2}^{T_f^{\text{trans}}} + \overbrace{\frac{1}{2}(F_{\overline{yy}}\dot{\chi}_f^2 + 2F_{\overline{yz}}\dot{\chi}_f\dot{\theta}_f + F_{\overline{zz}}\dot{\theta}_f^2)}^{T_f^{rot}} + \overbrace{J_f\dot{\phi}_f\chi_f\dot{\theta}_f + \frac{1}{2}J_f\dot{\phi}_f^2}^{T_{fwheel}^{spin}} \quad (2)$$

$$V_t = \left[m_r g\bar{h}_r + m_f g\bar{h}_f - \frac{g}{2}(m_t\bar{h}_t\chi_r^2 - 2\psi\chi_r\nu + \psi^2\sin\lambda\nu)\right]\cos\alpha + m_t g[h + (Y_r + \bar{l}_t)\sin\alpha] \quad (3)$$

$$T_t = T_f + T_r \quad (4)$$

where T_f, T_r, T_t is the kinetic energy of the front part, the rear part and the total system, respectively, and V_t is the total potential energy of the bicycle system.

The motion equations of the stability submodel have been derived in the form of Lagrange's equation. The application of this formalism automatically takes into account given constraints and at the same time guarantees that all interactions between forces are included. Now we introduce the Lagrange function L, as shown in

$$L = T_t - V_t \quad (5)$$

A set of seven equations of motion is derived from Lagrange's equation:

$$\frac{d}{dt}\left(\frac{\partial L}{\partial \dot{q}_j}\right) - \frac{\partial L}{\partial q_j} = F_j \quad (j = 1\ldots7) \quad (6)$$

where q_j is the jth generalized coordinate and F_j is the generalized force in the jth generalized coordinate. The derivation of F_j is outlined in Appendix A and is expressed by Eq. (A1)–(A7).

According the Eq. (6), we can derive the following seven motion equations:

$$F_{rY} - F_{fY} - F_{\text{drag}} - F_{\text{wind}} = m_t\ddot{Y}_r + m_t g\sin\alpha \quad (7)$$

$$M_{\text{drive}} - F_{rY}r - M_{rrt} - M_{\text{brake}} = J_r\ddot{\phi}_r \quad (8)$$

$$F_{fY}r - M_{frt} = J_f\ddot{\phi}_f \quad (9)$$

$$F_{rX} + F_{fX} = m_t\ddot{X}_r - m_t\bar{l}_t\ddot{\theta}_r + m_t\bar{h}_t\dot{\chi}_r - m_f d\ddot{\psi} \quad (10)$$

$$M_{\chi_r} = m_t\bar{h}_t\ddot{X}_r + T_{yz}\ddot{\theta}_r - S_t\dot{\theta}_r + T_{yy}\ddot{\chi}_r - gm_t\bar{h}_t\chi_r\cos\alpha + P_{\lambda y}\ddot{\psi} - S_f\cos\lambda\dot{\psi} + g\nu\psi\cos\alpha \quad (11)$$

$$-C_w F_{fX} = -m_t\bar{l}_t\ddot{X}_r + T_{zz}\ddot{\theta}_r + T_{yz}\ddot{\chi}_r + S_t\dot{\chi}_r + P_{\lambda z}\ddot{\psi} - S_f\sin\lambda\dot{\psi} \quad (12)$$

$$M_\psi + C_f F_{fX} = -m_f d\ddot{X}_r + P_{\lambda z}\ddot{\theta}_r + S_f\sin\lambda\dot{\theta}_r + P_{\lambda y}\ddot{\chi}_r + S_f\cos\lambda\dot{\chi}_r + g\nu\chi_r\cos\alpha + P_{\lambda\lambda}\ddot{\psi} - g\nu\sin\lambda\cos\alpha\psi \quad (13)$$

where $S_r = J_r\dot{\phi}_r$, $S_f = J_f\dot{\phi}_f$, $S_t = S_f + S_r$, $T_{yy} = m_r\bar{h}_r^2 + R_{\overline{yy}} + m_f\bar{h}_f^2 + F_{\overline{yy}}$, $T_{zz} = m_r\bar{l}_r^2 + R_{\overline{zz}} + m_f(C_w + \bar{l}_f)^2 + F_{\overline{zz}}$, $T_{yz} = -m_r\bar{h}_r\bar{l}_r + R_{\overline{yz}} - m_f\bar{h}_f(C_w + \bar{l}_f) + F_{\overline{yz}}$, $P_{\lambda\lambda} = m_f d^2 + F_{\overline{yy}}\sin^2\lambda - F_{\overline{yz}}\sin 2\lambda + F_{\overline{zz}}\cos^2\lambda$, $P_{\lambda y} = -m_f\bar{h}_f d - F_{\overline{yy}}\sin\lambda + F_{\overline{yz}}\cos\lambda$, and $P_{\lambda z} = m_f(C_w + \bar{l}_f)d - F_{\overline{yz}}\sin\lambda + F_{\overline{zz}}\cos\lambda$.

We assume enough friction exists between the tire and the ground so that there is no relative motion between the point of contact of the wheels and the ground. So after developing Lagrange's equation, we add four nonlinear rolling constraints to the stability submodel. The four constraints are as follows:

$$\dot{Y}_r = r\dot{\phi}_r\cos\theta_r \quad (14)$$

$$\dot{X}_r = -r\dot{\phi}_r\sin\theta_r \quad (15)$$

$$\dot{Y}_f = r\dot{\phi}_f\cos\theta_f \quad (16)$$

$$\dot{X}_f = -r\dot{\phi}_f\sin\theta_f \quad (17)$$

By assuming small angles of rotation the four nonlinear nonholonomic constraints reduce to four linear nonholonomic constraints. With the help of the rolling constraints, we reduce the number of generalized coordinates in the equations to three. In the bicycle simulator, the most important dynamics variables need to be simulated are Y_r, χ_r and ψ, so the final bicycle motion equations can expressed as follows:

$$\frac{M_{\text{drive}} - M_{\text{brake}} - M_{rrt} - M_{frt}}{r} - F_{\text{drag}} - F_{\text{wind}} - m_t g\sin\alpha = \left(m_t + \frac{J_f}{r^2} + \frac{J_r}{r^2}\right)\ddot{Y}_r \quad (18)$$

$$W_{\chi\chi}\ddot{\chi}_r + C_{\chi\chi}\dot{\chi}_r + K_{\chi\chi}\chi_r + W_{\chi\psi}\ddot{\psi} + C_{\chi\psi}\dot{\psi} + K_{\chi\psi}\psi + I_{\chi_r} = M_{\chi_r} \quad (19)$$

$$W_{\psi\psi}\ddot{\psi} + C_{\psi\psi}\dot{\psi} + K_{\psi\psi}\psi + W_{\psi\chi}\ddot{\chi}_r + C_{\psi\chi}\dot{\chi}_r + K_{\psi\chi}\chi_r + I_\psi = M_\psi \quad (20)$$

The coefficients of Eqs. (19) and (20) can be derived from Eqs. (7)–(17), and we do not list the expressions in the text because of terseness. A more detailed derivation process is outlined in CongChen [6]. In this form, the equations can be solved numerically with the help of standard methods like the Runge–Kutta method.

2.3 Vibration Submodel. The vibration submodel was developed with the intention to evaluate vibration response of a bicycle without wheel suspensions. In order to simplify the model, we make the following assumptions about the road-bicycle-rider system.

(1) The system is represented by a mechanical system with two rigid bodies linked together by revolute joints and translational joints, springs, and dampers. The rigid bodies refer to the rider and the central frame (including the front and rear wheel, derailleur, and other accessories). The spring and damper elements are used to model the tires of wheels, seat, and handlebar-arm section.
(2) The rider can only sit on the seat and never stand up which is very normal during common riding. The rider is treated as a rigid body connected to the seat by a revolute joint. Also the rider's hands never leave the handlebar, so the handlebar-arm section can be modeled as a spring-damper element.
(3) The tires of wheels are modeled as linear springs combined with linear viscous dampers. And the tire is inflated enough and there is only one point on a wheel in contact with the ground. Although this is the simplest modeling of a tire, it can basically describe the tire's physical characteristics, especially for a bicycle's narrow face tires.
(4) The only vibration excitation to system comes from the

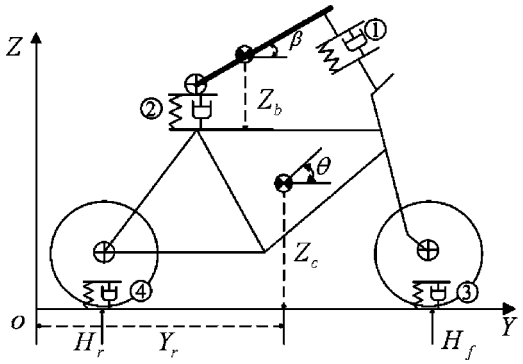

Fig. 6 Sketch of vibration submodel

unevenness road surface. The other vibration sources, such as pedaling and rider's maneuvers, are omitted.

According to these assumptions, our vibration submodel is simpler than Waechter's [7], Wilczynski's [8], and Wong's [9], but it is enough to predict vibration response for our bicycle simulator system. Combing with the real condition of the road, bicycle, and rider, a two-dimensional mathematical vibration model is formulated by Lagrange's equation.

A sketch of the submodel is shown in Fig. 6. The two rigid bodies are indicated by ⋈, the pivot points of the rider and the center frame are indicated by ⊕. The numbers in circles mark the spring-damper system in the model as follows: ① handle-arm section, ② seat, ③ front tire, and ④ rear tire. Basic parameters used to specify bicycle structure from the viewpoint of vibration are shown in Fig. 7.

Five independent generalized coordinates are used to describe the bicycle's position and configuration at any time: The coordinates Y_r, Z_c, and Z_b; and the angles β and θ. Similar to the stability submodel, we derive the dynamics equations of road-bicycle-rider system through Lagrange's equation.

First we derive formulas for the kinetic energy T, the potential energy V, and the dissipative function D as follows:

$$T=\frac{1}{2}M_b\dot{Z}_b^2+\frac{1}{2}J_b\dot{\beta}^2+\frac{1}{2}M_c\dot{Z}_c^2+\frac{1}{2}J_c\dot{\theta}^2 \tag{21}$$

$$V=\frac{1}{2}K_1(Z_b\cos\lambda+l_1\beta-Z_c\cos\lambda-l_3\,\theta\cos\lambda)^2+\frac{1}{2}K_3(Z_c+l_3\,\theta-H_f)^2+\frac{1}{2}K_4(Z_c-l_4\,\theta-H_r)^2+\frac{1}{2}K_2(Z_b\cos\lambda-l_2\,\beta\cos\varphi-Z_c+l_4\,\theta)^2 \tag{22}$$

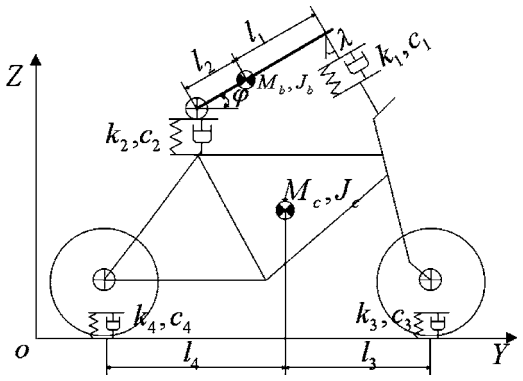

Fig. 7 Basic parameters of vibration submodel

Fig. 8 Instrumented bicycle and the potentiometer

$$D=\frac{1}{2}C_1(\dot{Z}_b\cos\lambda+l_1\,\dot{\beta}-\dot{Z}_c\cos\lambda-l_3\,\dot{\theta}\cos\lambda)^2+\frac{1}{2}C_3(\dot{Z}_c+l_3\,\dot{\theta}-\dot{H}_f)^2+\frac{1}{2}C_4(\dot{Z}_c-l_4\,\dot{\theta}-\dot{H}_r)^2+\frac{1}{2}C_2(\dot{Z}_b-l_2\,\dot{\beta}\cos\varphi-\dot{Z}_c+l_4\,\dot{\theta})^2 \tag{23}$$

Then, according to the theory of analysis mechanics, a set of motion equations is derived from Lagrange's equation:

$$\frac{d}{dt}\left(\frac{\partial T}{\partial\dot{q}_i}\right)-\frac{\partial T}{\partial q_i}+\frac{\partial V}{\partial q_i}+\frac{\partial D}{\partial\dot{q}_i}=0 \tag{24}$$

where q_i is the ith generalized coordinate.

The velocity of bicycle $\dot{Y}_r$ is solved in the stability submodel and just input to the vibration submodel to evaluate the road profile variables: H_f, H_r, $\dot{H}_f$, $\dot{H}_r$, so the number of motion equations is reduced to four. The final motion equations can expressed as follows:

$$[M]\{\ddot{z}\}+[C]\{\dot{z}\}+[K]\{z\}=\{F\} \tag{25}$$

where: $[M]$, $[C]$, and $[K]$ are mass matrix, damping matrix, and stiffness matrix, respectively, $\{z\}=\{Z_c,Z_b,\beta,\theta\}^T$ is the generalized coordinate vector, and $\{F\}$ is the excitation vector expressed by combination of road profile variables: H_f, H_r, $\dot{H}_f$, $\dot{H}_r$.

The element in the above matrix and vector can be derived from Eq. (24). Also, we can get numerical solutions for motion equations through the Runge–Kutta method.

3 Validation of the Model

Most studies on bicycle dynamics were purely theoretical ones. Although this kind of approach can accurately model the idealized behavior of a bicycle, only actual measurements of a real bicycle can reveal how the bicycle is balanced and vibrated during normal riding. We have done experiments to verify our stability submodel and vibration submodel, respectively. To validate the stability submodel, we have measured the steering angle ψ, tilt angle χ_r, and the velocity of bicycle $\dot{Y}_r$. To verify the vibration submodel, we have measured the road profiles and corresponding vibration accelerations at several positions of rider-bicycle system. These measurements are enough to verify the above two models. The road profile will be discussed in detail in Sec. 4.3.

3.1 Instrumented Bicycle. According to the requirements of validation, we have set up an experimental bicycle mounted with several kinds of instruments, as shown in Fig. 8. With the help of this experimental bicycle, we can measure those variables during normal riding. The data were acquired from four sensors using a laptop computer with 12-bit USB data acquisition card. The rider carried the computer in a small bag. Data was acquired through

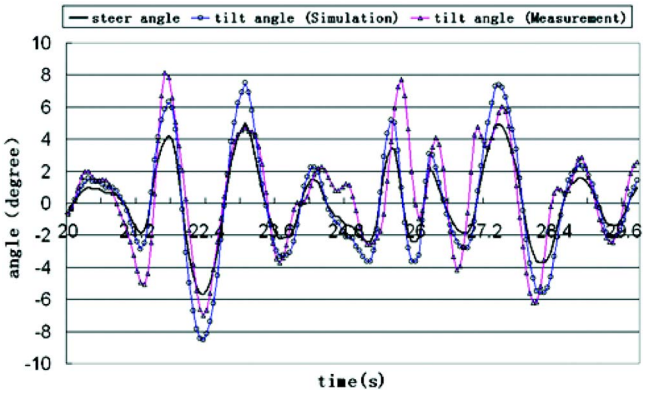

Fig. 9 Comparison of tilt angle

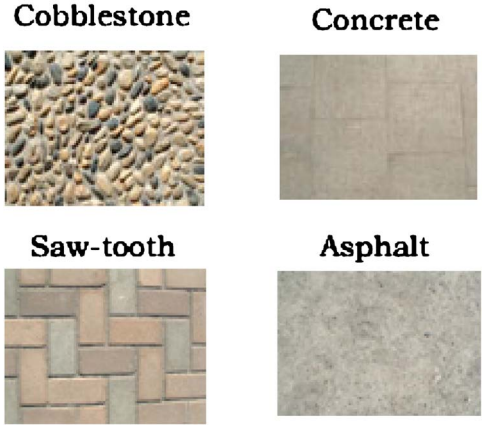

Fig. 10 Measured road profiles

four channels at 100 kHz.

To measure the velocity, a transducer from a commercially available cyclometer was used. To measure the tilt angle, an AccuStar® angle transducer was mounted to the frame center and was within the plane of the frame. To measure the steering angle, a low-noise high linearity potentiometer was used. The potentiometer was mounted on a bracket (as shown in Fig. 8), and recorded the steering angle of the handlebars through the movement of a pair of gears.

The vibration accelerations were measured through an acceleration transducer. Through changing its mounting position, we acquired the vibration accelerations at the handlebars, the seat, and the center frame. The road profiles were also measured through the AccuStar® angle transducer, which was mounted within the plane of the frame. When the bicycle was pushed slowly along a marked line on the road surface, the sensor recorded the pitch angle data caused by the road profile at the contact point between the wheel and the road, and then converted the pitch angle into the road profile data.

3.2 Validation of Stability Submodel. This submodel depends upon the time-independent steer angle, tilt angle, and the velocity of a bicycle. Because of the limitation of our instruments, the experimental data were acquired when the rider was riding in a nearly straight line on a very even road. During the riding, the rider hardly controlled the handlebar and was skillful enough to keep the bicycle very stable. The bicycle had an idealized steering and tilting behavior, so both the steer torque and tilt torque are equal to zero. Afterward, the steer angle is input into the stability submodel, a comparison of tilt angle between the numerical simulation result calculated from the stability submodel and measurement result is displayed in Fig. 9 (the velocity of the bicycle is 3.5 m/s). The simulation parameters of the submodel are outlined in Appendix B.

Based on Fig. 9, the simulation result is of the same variation trend with the measured result. It shows that the bicycle has some degrees of self-stability. And we also found that the results are in accord with that of Lowell's [3] and Hand's [5], namely, the tilt angle is proportional to the lean angle at the given velocity range as shown in the following equation:

$$\chi_r = k\psi \ (k = \text{const}) \tag{26}$$

In Figure 9, there are several differences between the simulated and the measured tilt angle such as t=24.8 s, 27.2 s which the measured tilt angle accord with Eq. (26). We assumed that the experimental road was even and the rider did not control the handlebars, but in the real measurement the road was uneven and the rider should steer the handlebars slightly sometimes in order to keep the bicycle stable.

3.3 Validation of Vibration Submodel. As mentioned above, in order to verify the vibration submodel, we have measured the road profiles and corresponding vibration accelerations at several positions of a rider-bicycle system. Vibration data consist of a time series of the accelerations measured at the handlebar, the seat, and the frame center. Vibration measurements have to be taken for a very long distance in order to collect as much data as possible for each specific road profile. Because the measurements of the vibration accelerations and the road profile do not happen at the same time, and it is not possible to find the vibration data which precisely match the road profile, the acceleration data that are the closest to road profile are chosen for comparison.

We have gathered four kinds of road profiles that are very common in daily cycling: Cobblestone pavement, concrete pavement, saw-tooth pavement, and asphalt pavement. Figure 10 shows the four kinds of measured road profiles. Using the road profile and the bicycle velocity as the inputs, we can get the vibration response of the vibration submodel. The simulation parameters of the submodel are outlined in Appendix C. Figure 11 shows the comparison results of the acceleration amplitude at the bicycle frame center between simulated acceleration and measured acceleration under the same saw-tooth pavement. The results are compared in frequency spectra.

Figure 11 shows that the frequency response of the acceleration is in the range from 0 to 50 Hz. This interval of frequency range contains all significant parts of the acceleration. As mentioned above, the riding track of the vibration accelerations measurement is close but not identical to the measured road profile, the acceleration spectra cannot be expected to agree perfectly. But within the most important frequency ranges of about 8–14 Hz and 22–26 Hz, the acceleration spectra show good correspondence between simulation and measurement.

Using the rating of ride comfort is another way to validate our

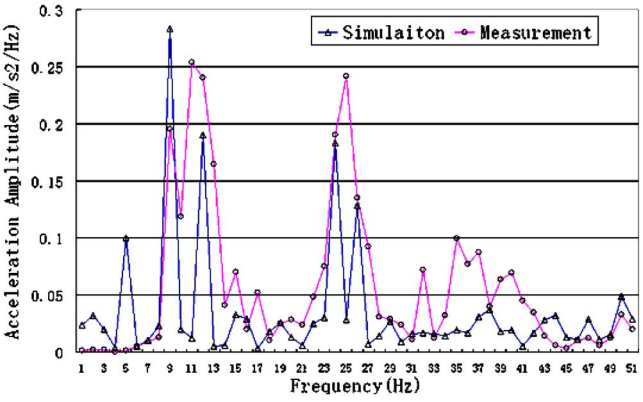

Fig. 11 Comparison of acceleration at the frame

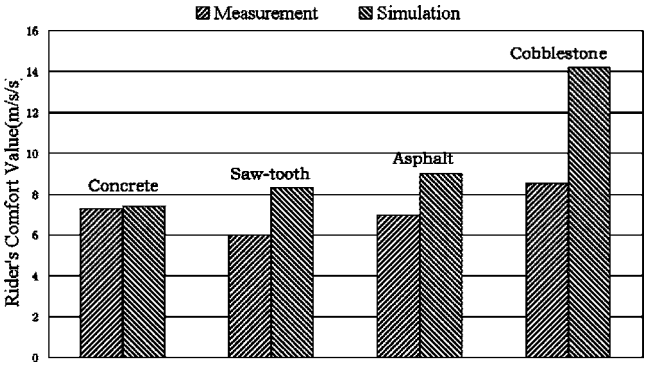

Fig. 12 Comparison of the ride comfort

vibration submodel which is very popular in the automobile dynamics analysis. The procedure is based upon recommendations provided in International Standard 2631 (1997) for quantifying whole-body vibration to assess human response. The data frequency spectra of simulation and measurement can be transformed into weight vibration intensities with the help of a weight function table from ISO2631 [10]. We have done ride comfort comparisons including four kinds of measured road profiles.

The comparison of ride comfort between measurement and simulation are shown in Fig. 12. On the concrete, measurement and simulation correspond rather well. On the saw-tooth and asphalt, the simulation is a little too high. It can be summarized that the correspondence between simulation and measurement is rather good, except for very uneven cobblestone.

4 Integration With the Bicycle Simulator

When the BDM was integrated with the interactive bicycle simulator system, some key input parameters must be determined first, such as rider's tilt torque, pedal torque, and the road profile data. According to the hardware configuration of the bicycle simulator, we can evaluate these parameters through the following methods.

4.1 Rider's Tilt Torque. According to our riding experience, the tilt torque is very important to balance the bicycle. For example, a rider can manage to have a left/right turn almost solely by leaning his/her body. In order to simulate this kind of behavior of the rider on the simulator, the BDM should get the tilt torque of the rider in real time. A motion tracker is used to fix to the rider's back, so as to measure the rider's lateral lean angle in real time. The motion tracker is a sensor that can get the position and orientation of a moving object [11]. As the lean angle is known, we can easily get the tilt torque in real time.

4.2 Rider's Pedal Torque. The interactive bicycle simulator requires the information of the bicycle's absolute position for rendering the virtual scene and determining bicycle collision with obstacles, such as ground and guardrail. In the BDM, the generalized coordinate Y_r describes the position of the bicycle. According to the Lagrangian method, the generalized forces along the generalized coordinate Y_r are rider's pedal torque, wind drag force, rolling friction resistance, etc (Appendix A). In our simulation, the wind drag force is proportional to the square of the bicycle velocity, as shown in the following equation:

$$F_{\text{drag}} = \frac{1}{2}\rho c_d v^2 A \tag{27}$$

where ρ is the air density, c_d is the drag coefficient, ν is the bicycle velocity, and A is the frontal area of the bicycle system.

The rider's pedal torque M_{rider} is difficult to measure precisely on the simulator, because the force exerted on the pedal is nonuniform during the rotation of the pedal crank. So we use a software torque estimator to evaluate the rider's pedal torque in real time. The torque estimator is based on the dynamics of the rear wheel hardware system which can be expressed as

$$M_{\text{rider}} - M_{\text{motor}} = I_r \varepsilon_{rw} \tag{28}$$

where M_{motor} is the torque of the motor (the feedback force of the pedal, either positive or minus), and I_r is the inertia of the pedal system.

Since we can measure the acceleration ε_{rw} through the photoelectric encoder mounted on the bicycle simulator, and know M_{motor} from the previous sampling step, the rider's torque can be estimated as

$$M_{\text{rider}} = I_r \varepsilon_{rw} + M_{\text{motor}} \tag{29}$$

With M_{rider}, the stability submodel can calculate the absolute position of virtual bicycle in the virtual scene and the new feedback force of pedal resistance motor M_{motor}.

4.3 Road Profile. In the BDM, the road profile is an important input data because it influences both the stability submodel and the vibration submodel. A profile is a two-dimensional slice of the road surface, taken along an imaginary line; commonly we refer to this line as the longitudinal profiles [12]. The road profile can be divided into the low-frequency (LF) component and high frequency (HF) component. The LF indicates whether the road is going up, going down, or keeping horizontal. The HF indicates the deviation from the smooth profile.

In the interactive bicycle simulator system, the LF (together with the gradient) can get through collision detection from the visual scene. The virtual bicycle is bound with a line segment which is used to do collision detection with the ground in the visual scene. The collision detection returns the normal vector of the collision point which can be used to evaluate the LF. The HF cannot get from the visual scene, so we must construct a road profile database which consists of different road surface data. According to the road surface on which the virtual bicycle is running on, the corresponding road profile data can be queried from the database in real time.

As mentioned above, we have measured four kinds of road profiles. Our database mainly come from these experimental data, while some data are constructed artificially according to the virtual scene. In order to get HF from the experimental data, we filter the experimental data in moving average [12], which can be formulated as follows:

$$p_{fH}(i) = p(i) - \frac{1}{N}\sum_{j=i-\frac{B}{2\Delta X}}^{i+\frac{B}{2\Delta X}} p(j) \tag{30}$$

Where $p_{fH}(i)$ is the high frequency profile, B is the base length of the moving average, ΔX is the interval of sample, p is the original sampled profile, and N is the number of samples included in the summation.

5 Conclusions

An innovated completed mathematical model of a bicycle was presented. The model consisted of two slightly coupled submodels, namely, the stability submodel and vibration submodel. These two submodels described the bicycle's stability and vibration behavior, respectively. The motion equations were developed based on the Lagrange's equation, and also the Runge–Kutta method was selected to make numerical simulation. We did experiments to validate our mathematical model, and revealed that the results of numerical simulation of our model were basically in accord with the experiment data. Also, we put forward methods to evaluate the tilt torques and pedal torque of the rider, and processed the road profile data in the bicycle simulator system.

The above full bicycle model and the data processing methods have been successfully integrated to the whole bicycle simulator

system (Fig. 2). The rider can maneuver the bicycle simulator with the same maneuvers as a real bicycle, and get a very realistic riding feeling.

Acknowledgments

This work is a result of the project "Research on Key Technologies of VR System in Unix Operation System and their Applications" (No. 025115007), which is supported by the Ministry of Science and Technology of Shanghai, China. Furthermore, thanks are also given to Cong Chen and Baichuan Fu for assisting in the experiments. Thanks are also given to Falk Riess for private communications.

Nomenclature

- ε_{rw} and ε_h = the angular acceleration of rear wheel and handlebar, respectively;
- H_f and H_r = the road profile of the front and rear wheel contact point with the ground, respectively;
- α = the road gradient;
- M_{driver}, M_ψ, and M_{χ_r} = the pedal torque, steer torque and tilt moment put on by the rider, respectively;
- M_{pm} and M_{hm} = the torque of the motor of rear wheel and handlebar force feedback system, respectively;
- X_r and Y_r = the position coordinates of rear wheel contact point with the ground;
- X_f and Y_f = the position coordinates of front wheel contact point with the ground;
- χ_r and χ_f = the tilt angle of the rear frame and the front frame from the vertical frame, respectively;
- θ_r and θ_f = the heading angle of the rear frame and the front frame from the longitudinal axis, respectively;
- ψ = the rotation angle of handlebar;
- ϕ = the lean angle of the rider on the simulator;
- ϕ_f and ϕ_r = the angular position of the front and rear wheels, respectively;
- Z_c = the vertical position of the central frame's gravity center relative to ground;
- Z_b = the vertical position of the rider trunk's gravity center relative to saddle spring;
- β = the angle between the rider trunk and central frame; and
- θ = the angle between the central frame and the inertial reference frame of the ground.

Appendix A: Generalized Forces

When the bicycle was running along the XY plane (ground surface), the generalized forces acted on the rider-bicycle system (Figs. 13 and 14).

G is the gravity of the rider-bicycle system, N_r and N_f are the constraint force on the rear and front wheel, respectively, F_{rY} and F_{fY} are the constraint forces on the rear and front wheel, respectively, initially in the Y direction, F_{rX} and F_{fX} are the constraint forces on the rear and front wheel, respectively, initially in the X direction, M_{rrt} and M_{frt} are the rolling friction resistance on the rear and front wheel, respectively, F_{wind} and F_{drag} are the wind resistance and drag forces on wheels, respectively, M_{drive} and M_{brake} are the pedaling torque and the braking torque acting by the rider, respectively, and M_ψ and M_{χ_r} are the steer torque and the tilt torque acting by the rider, respectively.

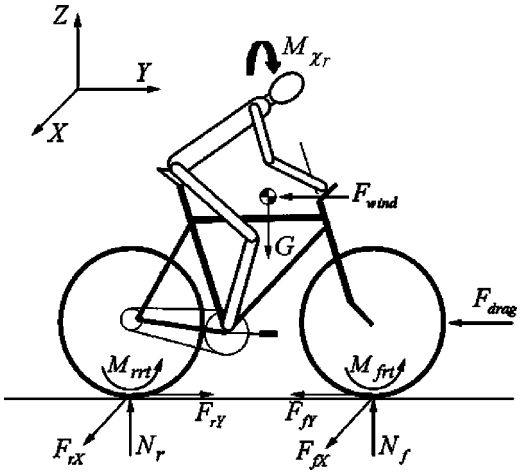

Fig. 13 Forces acting on the rider-bicycle system

These generalized forces can be formulated as the following equation. The coordinate to which each generalized force belongs is indicated by the subscript of the generalized force.

$$F_{Q_{Y_r}} = F_{rY} - F_{fY} - F_{\text{drag}} - F_{\text{wind}} \tag{A1}$$

$$F_{Q_{\phi_r}} = M_{\text{drive}} - F_{rY}r - M_{rrt} - M_{\text{brake}} \tag{A2}$$

$$F_{Q_{\phi_f}} = F_{fY}r - M_{\text{frt}} \tag{A3}$$

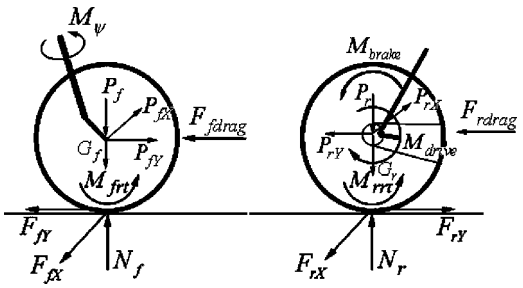

Fig. 14 Forces acting on the front and rear wheel respectively

$$F_{Q_{X_r}} = F_{rX} + F_{fX} \tag{A4}$$

$$F_{Q_{\theta_r}} = -C_w F_{fX} \tag{A5}$$

$$F_{Q_{\chi_r}} = M_{\chi_r} \tag{A6}$$

$$F_{Q_{\psi}} = M_{\psi} + C_f F_{fX} \tag{A7}$$

Appendix B

Main simulation parameters of the stability submodel

	Model parameter	Initial value	Source
Rear part	m_r: Mass	m_r=90 kg	Measured
	$\bar{l}_r$: Horizontal position of mass center	$\bar{l}_r$=0.508 m	
	$\bar{h}_r$: Vertical position of mass center	$\bar{h}_r$=1.27 m	
Front part	m_f: Mass	m_f=5.0 kg	Measured
	$\bar{l}_f$: Horizontal position of mass center	$\bar{l}_f$=−0.1236 m	
	$\bar{h}_f$: Vertical position of mass center	$\bar{h}_f$=0.7558 m	
Wheel	r: Radius of wheel J_r,J_f: Moment of inertia of wheel	r=0.33 m J_r,J_f=0.2 kg*m^2	Measured Derived
Others		Ref. [5]	

Appendix C

Spring-damper system parameters of the vibration submodel

	Model parameter	Initial value	Source
Handlebar arm	K_1: Stiffness C_1: Damping	K_1=14 900 N/m C_1=202 N s/m	Ref. [7]
Seat	K_2: Stiffness C_2: Damping	K_2=48 650 N/m C_2=1000 N s/m	
Tire	K_3, K_4: Stiffness C_3, C_4: Damping	K_3, K_4=134 000 N/m C_3, C_4=272 N s/m	Ref. [9]
Others		Ref. [7]	

References

[1] Kwon, D.-S., Yang, G.-H, et al. 2001, "KAIST Interactive Bicycle Simulator," *Proc., IEEE International Conference on Robotics and Automation*, IEEE, NY, Vol. **3**, pp.2313–2318.

[2] Jones, D. E. H., 1970, "The Stability of the Bicycle," Phys. Today, **23**, pp.34–40.

[3] Lowell, J., and McKell, H. D., 1982, "The Stability of Bicycles," Am. J. Phys., **50**(12), pp.1106–1112.

[4] Fajans, J., 2000, "Steering in Bicycle and Motorcycles," Am. J. Phys., **68**(7), pp.654–659.

[5] Hand, R. H., 1988, "Comparisons and Stability Analysis of Linearized Equations of Motion for a Basic Bicycle Model," M.S. thesis, Cornell University, Cornell, NY.

[6] Chen, C., 2004, "A Study of Dynamic Modeling of Interactive Bicycle Simulator Based on Virtual Reality," M.S. thesis, Shanghai Jiaotong University.

[7] Waechter, M., and Riess, F., 2002, "A Multibody Model for the Simulation of Bicycle Suspension Systems," Veh. Syst. Dyn., **37**(1), pp.3–28.

[8] Wilczynski, H., and Hull, M. L, 1994, "A Dynamic System Model for Estimating Surface-induced Frame Loads during Off-Road Cycling," J. Mech. Des., **116**, pp.816–821.

[9] Wong, M. G., and Hull, M. L., 1983, "Analysis of Road Induced Loads in Bicycle Frames," ASME J. Mech., Transm., Autom. Des., **105**, pp.138–145.

[10] Torbic, D. J., 2001, "Comfort and Controllability of Bicycles as a Function of Rumble Strip Design," Ph.D. thesis, The Pennsylvania State University.

[11] *The Flock of Birds® Installation and Operation Guide*, 1999, Ascension Technology Corporation.

[12] Sayers, M. W., and Karamihas, S. M, 1998, "*The Little Book of Profiling*," University of Michigan.